lajss.org Latin American Journal of Solids and Structures
www.lajss.org

Mechanical and structural optimisation of transverse and radial load bearing characteristics of reed straw based on finite elements

Guoyu li[a*] https://orcid.org/0000-0002-2372-6512, **Xuanhao cui** [a]

[a] School of Mechanical Engineering, Shanghai Dianji University, Shanghai, 201306, People's Republic of China. Email: ligy@sdju.edu.cn, xuanhaocui@qq.com

* Corresponding author

Abstract

Straw, as a widely available agricultural by-product, has a variety of excellent properties such as good mechanical properties, sustainability, and low cost, which makes it valuable to study in different fields of research and applications. In this study, the mechanics of lateral and radial load-bearing characteristics of reed straw were investigated. The research focused on structural optimization using Micro-CT (Micro-Computed Tomography) and Mimics inverse reconstruction techniques, Finite element analysis was employed in the study. The method involved comparing the mechanical properties of the real model of straw with those of the optimized model. Micro-CT scanning technology was used to obtain the cross-section image data of reed straw, and the image data were processed by Mimics software to generate three-dimensional geometric models of the outer skin, vascular bundles and inner foam core. The finite element analysis method was used to set the material properties and loading conditions, and a finite element simulation model of the straw was established to investigate the mechanical properties of reed straw under axial and radial compression conditions. In order to facilitate the biomimetics design of reed straw, the mechanical properties of the real model and the optimised model were simulated and compared. It was found that the nodal features maintained the structural stability by providing radial constraints on the outer bark and pith core of the straw under both axial and radial compression, and the internal vascular bundles of the straw played a key role in the axial and radial compression of reed straw. The microstructure of vascular bundles was found to be scattered in the basic tissues with gradually increasing size and decreasing number, and their distribution uniformity and density directly affects the overall mechanical properties of the straw. The stress distribution between the real model and the optimised model of straw was relatively uniform, with the maximum stress value of 64.59 MPa in axial compression and 1.17 MPa in radial compression for the real

model, indicating that there is a significant difference in the axial and radial load-bearing capacity of straw. The maximum stress usually occurs at the nodes, which is the most vulnerable site of failure in straw and plays an enhanced role in structural stability. Therefore, this study reveals the mechanical response mechanism of reed straw under different compression conditions, which provides an important reference for future research and application of bio-materials.

Keywords

Reed straw; 3D reconstruction; Finite element analysis; Axial compression; Radial compression

Graphical Abstract

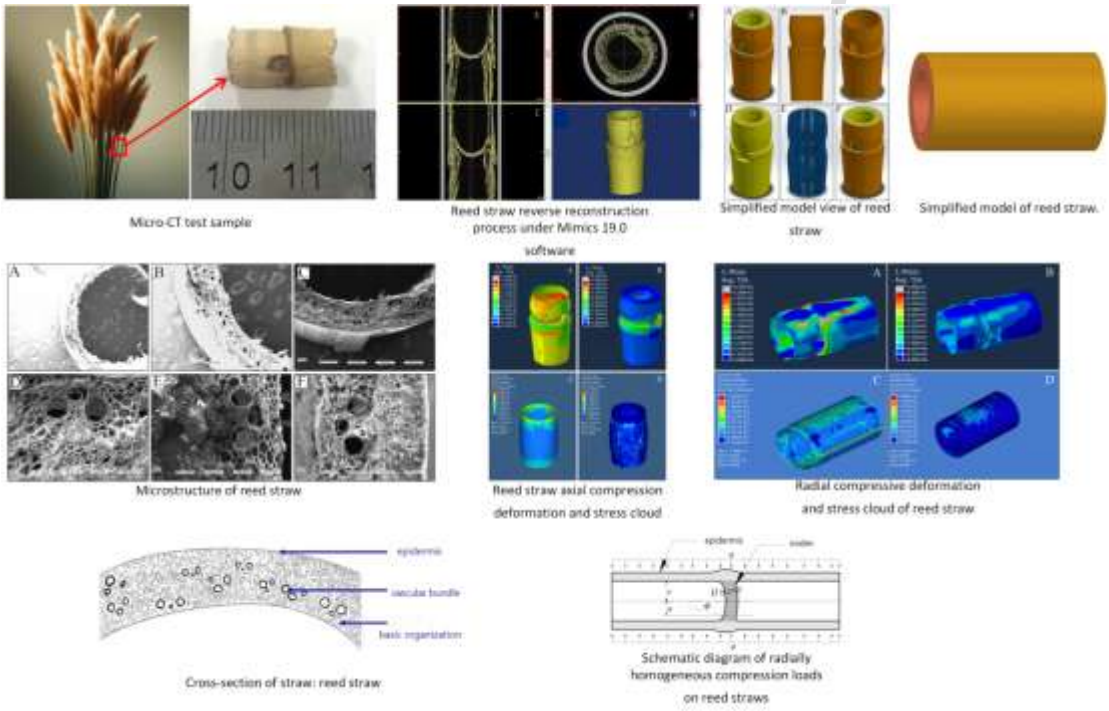

1 INTRODUCTION

With the rapid development of global agricultural production and scientific and technological progress, crop residues, as an important renewable resource, have attracted extensive attention from the scientific research and industrial communities.(Cheng et al. 2013) Crop straw is not only a renewable biomass resource, but also an important renewable resource. Crop straw is not only a renewable biomass resource, but also has the characteristics of biodegradability and resource recycling(Feng et al. 2011). Crop straw is recognized not only as a renewable biomass resource but also as having the characteristics of biodegradability and recyclability. In the fields of material science, biomedicine and environmental science, straw-based materials have shown their unique advantages and wide application prospects(Yin et al.). In particular, the study of its microstructure and mechanical properties(SHON et al. 2019) provide an important theoretical basis and technical support for the further development and application of straw-based materials.

Reed straw, as one of the typical crop stalks, has been widely studied for its unique structural and mechanical properties(Song et al. 2020). Its unique vascular structure and cellular composition give it excellent compressive and flexural properties in terms of mechanical properties, which makes it an ideal candidate for bionic engineering, lightweight structural material design and other fields(RISÉN et al. 2013). These properties make it an ideal candidate for bionic engineering and lightweight structural material design.

In recent years, the mechanical properties of Dyson et al. measured the physical properties, tensile strength, shear strength and modulus of elasticity of wheat straw (var Mercia) internode stems in a series of experiments. It was concluded that plant maturity had a significant effect on shear strength, which was highest at the beginning of maturity, and that Young's modulus increased with maturity, but had no effect on the modulus of rigidity(O Dogherty et al. 1995). Wang Shuai et al. tested the mechanical properties of fresh corn stover by means of a universal testing machine, obtained load displacement curves, and obtained data on relevant mechanical parameters, and established a mechanical model using the theory of composite mechanics. It was found that the required compression force of the stalks was greater than the required bending force, and the compression force required for nodulated stalks was greater than that for non-nodulated stalks(Wang et al. 2018) Regragui et al. developed a 3D model in Catia V5 by adding straw fibres and carried out mechanical tensile tests, the results obtained were found to improve the mechanical properties of earth bricks, indicating that straw fibres can enhance the mechanical properties of the structure(S. Regragui et al. 2023). Bavan et al. processed corn fibre composite beams using hand lay-up method, finite element analysis using ANSYS software and modelling the material with appropriate assumptions. The fibres were subjected to morphological analysis and X-ray diffraction analysis by scanning electron microscopy (SEM) and X-ray diffractometer (XRD). From the results, it was found that the fabricated composite beams can be used for structural engineering applications(Bavan S et al. 2013). These studies not only deepen the understanding of the mechanical properties of plant straw, but also provide a scientific basis for its potential in engineering applications.

In a macro-micro study on straw, Song et al. studied sorghum and reed, two node-containing straw plants, and compared the main characteristics of sorghum and reed stalks using methods such as macroscopic observation and material composition analysis.The results showed that the functional groups of sorghum and reed stalks are basically similar, and the distinguishing features of sorghum stalks include a higher taper and a slightly greater reduction in wall thickness compared to reed stalks. The cross-section of sorghum straw was filled with pith structure, whereas reed straw has a hollow structure. Vascular bundles of sorghum are usually arranged in pairs, whereas those of reed are arranged in odd numbers. This study provides valuable insights into the field of biomechanics(Song et al. 2024) Han et al. obtained the structural characteristics of bamboo wall layers along the thickness and height directions by analysing the chemical composition, gradient structure, pore structure and hollow structure with variable cross-section of bamboo, and summarised the research progress of novel composites and structural components, which will provide a reference for future research in biomass biomimicry(Han et al. 2024). The research progress of novel composites and structural components was summarised and obtained, providing reference for future research in biomass bionics. These studies further deepen the understanding of the macroscopic and microstructural properties of straw plants and demonstrate the potential

of straw and other natural materials in the development of novel composites and structural components.

So far, the research on straw mainly focuses on the chemical composition and constituent elements, and less research on the mechanical properties and macro-microstructure of straw. The only studies are also mainly on sorghum, maize, wheat and other straws, and less on reed, so there is a lack of research on the mechanical properties and macro-microstructure of straw. Therefore, further research on the mechanical properties and macro-microstructure of reed straw is conducive to a comprehensive exploration of straw properties and lays the theoretical foundation for later engineering bionic applications.

The motivation for this research arises from the need to better understand the mechanical properties of plant materials like reed straw, which have potential applications in materials science, structural engineering, and bioengineering. In this study, accurately reconstruct the reed straw's microstructure and identify the elastic properties of its outer cortex and pith core, develop simulation models to predict its mechanical behavior under different compression conditions, and analyze the role of its nodal structures in enhancing mechanical performance.

The novelty of this research lies in the high-resolution digital modeling of reed straw's internal and external structures, with a particular focus on the nodes that are critical to its mechanical integrity. By integrating Micro-CT imaging with finite element analysis, this study provides a comprehensive understanding of how reed straw's unique anatomical features influence its strength and failure behavior. The findings contribute to the field of plant biomechanics and offer valuable insights for the development of bio-inspired materials with enhanced load-bearing capabilities.

2 MATERIALS AND METHODS

2.1 Sample

The reed samples used in this study were collected from uncontaminated farmland in Shandong Province, China. Reeds, a perennial herbaceous plant from the Gramineae family(Fu et al. 2023) , were gathered early in the morning to minimize water evaporation and preserve their natural state Qin et al. 2011. After collection, the samples were thoroughly rinsed with water to remove surface dust and impurities.Subsequently, the reeds were air-dried at room temperature (20–25°C) and a relative humidity of 40–60% for a period of 5 days. This drying process ensured a stable moisture content. The final length of the selected reed samples was approximately 1 m, with the section near the node, extending both inside and outside, being cut to a length of approximately 15 mm for detailed structural analysis.

After drying, the reeds were cleaned to remove any remaining debris, cut into uniform dimensions for testing, and stored in a climate-controlled environment to prevent moisture fluctuations prior to mechanical testing. This ensured that the reed samples reached an equilibrium moisture content, providing consistent and reliable conditions for subsequent analyses. The results are shown in Figure 1.

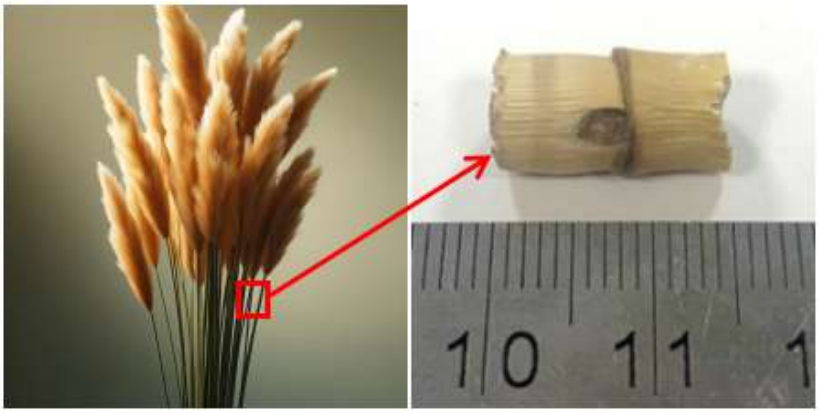

Figure1 *Micro-CT test sample.*

In this study, multiple analyses were conducted to ensure the reliability and repeatability of the results. Mechanical tests for axial and radial compression were performed on reed samples, with tests repeated on different days. The results showed minimal variation, indicating good repeatability.

Afterwards, the complete nodal and internodal structures were analysed. Detailed measurements and observations of the microstructure of the nodes and internodes were carried out in the laboratory using a microscope with a graduated scale to ensure that the internal structure and cellular arrangement could be accurately described.

2.2 Straw tomography scanner

CT scans are tomographic scans, which are completed with a series of non-overlapping cross-sectional image data of the sample. The image data acquisition equipment in this paper was a medical microcomputer tomography (μCT50, Scanco Medical AG, Switzerland). The resolution was 0.5 μm/μCT50, X-ray bulb voltage maximum 90 kVp, focal spot diameter 5-30 μm, maximum power 18 W, radiation dose to the outer surface of the device <0.25 μSv/h, resolution <2 μm (10% MTF), rated at 0.5 μm. detector system (CCD, 3400× 1200), electronic data acquisition. Maximum scanning size 50× 120 mm, maximum scanning sample size 100× 160 mm.

2.3 Observation of straw macro-microstructure

In this paper, a scanning electron microscope (SEM, Model EVO-18) manufactured by Zeiss, Germany, was used for microstructural analyses.The main parameters of the SEM are as follows: the accelerating voltage is usually adjustable from 1 KV to 30 KV, and the range of experimental magnification is from 13 to 50,000 times, with a minimum resolution of up to 3.0 nm.The samples were adequately processed prior to SEM experiments, including preparation, gold spraying treatment, mounting to the SEM stage, image acquisition and data processing. The outer epidermis and medullary core parts of the straw was cut by liquid nitrogen freezing, and the clear microscopic images were obtained after voltage and current adjustments, etc., so as to facilitate performance analysis and application.

2.4 Three-dimensional modelling of straw

2.4.1 Reverse reconstruction of medical images

The inverse modelling was carried out using the image data obtained from the CT scanning, and the three-dimensional model was established by the software Mimics, including the three-dimensional geometric model of the outer skin of the straw, the vascular bundles and the inner

foam core. The CT tomographic images of the straw were imported into Mimics19.0, and the "CT compressed image" method was selected, and the images were imported successfully after setting the orientation of the images(Ali et al. 2016). The import is successful. After importing the original medical image data, Mimics will automatically calculate and generate three views, front view, side view and top view (Figure 2 A-C). The images of these three positions are displayed. And they are related to each other for a series of preprocessing operations, including adjusting the window width, adjusting the contrast of the enhanced image and checking layer by layer to remove the surrounding noise, and finally obtaining the inverse reconstruction model (**Erro! Fonte de referência não encontrada.** D).

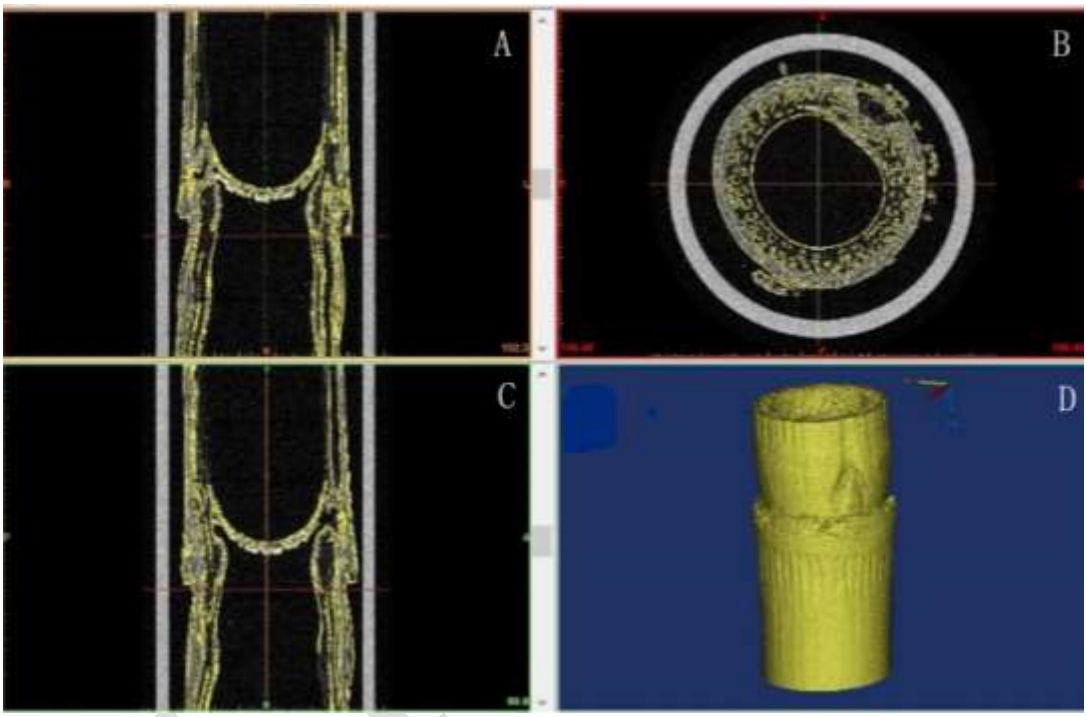

Figure2 *Reed straw reverse reconstruction process under Mimics 19.0 software (A) front view; (B) side view; (C) top view; (D) reverse reconstruction model.*

3 SIMULATION MODEL CONSTRUCTION AND CONDITIONS

3.1 Three-dimensional model construction

In this paper, the direction of internal vascular bundles and the distribution of fibres can be roughly observed by using Mico-CT(Li et al. 2015), but detailed cross-sectional features cannot be obtained, especially the structural features at the node part of the straw cannot be obtained. Combined with the SEM method, the internal structure obtained by reed straw can be finely obtained, thus facilitating the establishment of fine structural features of reed straw, which is closer to the biological prototype.

Based on fine structural features, reverse reconstruction is performed, with similar repair functions such as grid doctor, manifold creation, feature removal, and precise surface in Geomagic software (Luo et al. 2024) To combine the discontinuous noise information in each layer in the reconstructed model, so as to construct the complete and continuous 3 D model information, and establish the real model of reed straw was built in Solidworks 3D software by merging the

discontinuous noise information in each layer of the reconstructed model, so as to construct a complete and continuous 3D model information. By simplifying the real model, it was easy to carry out the subsequent finite element analysis, and its three views are as follows

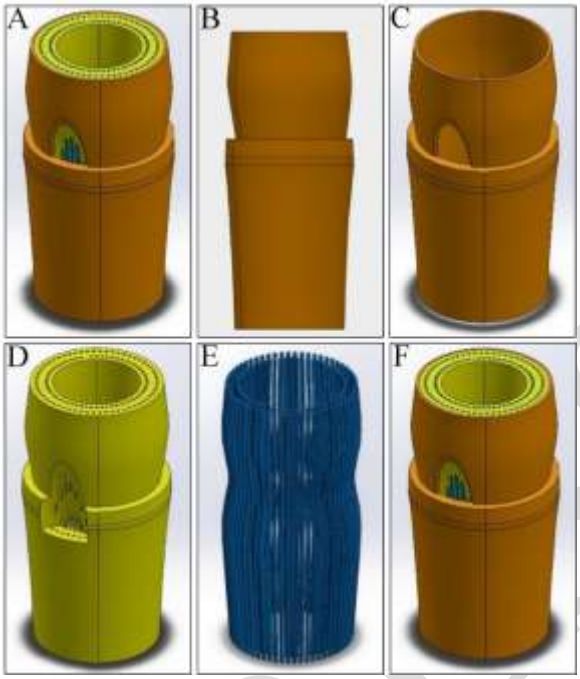

Figure A, C) shows. The reed straw mainly consists of the outer skin, foam matrix and vascular bundles of similar sizes, as shown in

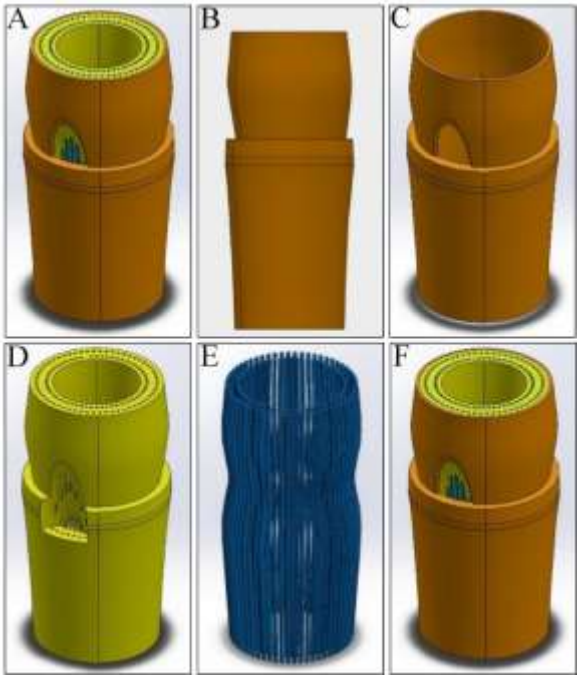

Figure D, F) shown. The outer bark shows stepwise thickening and outgrowth at the nodes; the tissue of the foam matrix was structurally adapted to the outer bark and has a more homogeneous texture; and the tissue of the fibrous vascular bundles was not completely straight, and the vascular bundles are more straight at the inter-nodal position, with flexure occurring at the nodes.

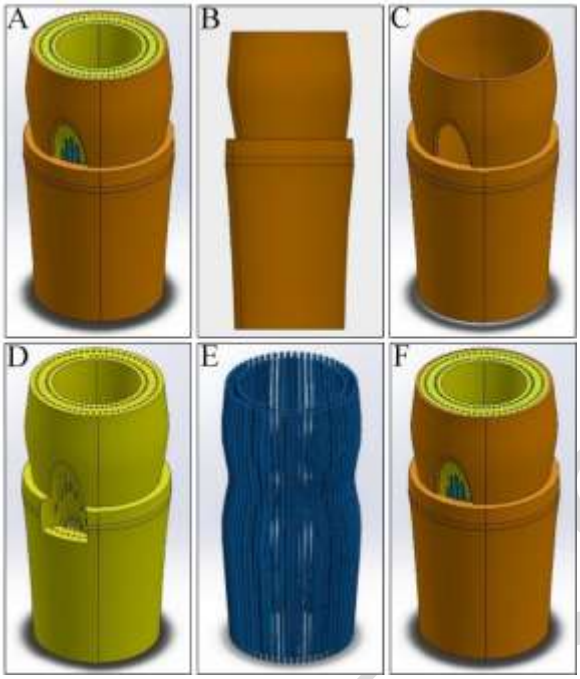

Figure 3 *Simplified model view of reed straw (A) Axonometric view of the overall model (B) Front view of the overall model (C) Right view of the overall model (D) Outer bark (E) Foam matrix (F) Vascular tissue.*

3.2 Three-dimensional simplified model construction

In order to compare with the 3D composite model and for subsequent engineering applications, a simplified model of reed straw was established in this paper(Huang et al. 2023), was shown in Figure 4. The nodal features are omitted from the simplified model, which was regarded as a regular cylinder with a through-straight structure consisting only of the outer bark and pith core.

For the axial and radial compression analysis of the model, according to the axial compression test of the stalk, it can be seen that the intercepted section of the stalk will fail when axial and radial compression of up to 25% is carried out under the Mechanical Universal Testing Machine (MUTM), i.e., the strain in excess of the elastic deformation is 30%, therefore, it is only compressed to 20% here.

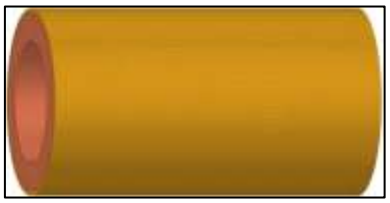

Figure 4. *Simplified model of reed straw.*

3.3 Simulation parameters and conditions

3.3.1 Material properties

Organismal tissues are composed of different cells, intercellular matrix and other microstructures(Yan et al. 2024) and the mechanical properties of their structures are non-uniform, non-linear and anisotropic(Schwaiger et al. 2024). The mechanical properties of biological tissues are non-uniform, non-linear and anisotropic. Currently, in the field of biomechanics,

research was carried out to approximate the segmentation of biological tissues into structurally homogeneous, isotropic as well as anisotropic materials(Yi et al. 2024). In this paper,anisotropic materials are used, which are closer to biological tissues. Through experimental measurements, combined with sugarcane(Yan et al. 2024) , wheat(Ingrīda et al. 2021.EWA G G C A M et al. 2011) wood(Kuai et al. 2024) and oilseed rape(Tamás et al. 2015) The elastic constants of reed straw were determined to be E1,E2,E3 by comparing the calculated elastic constants of the stalks.

A total of nine elastic parameters are involved in the straw bark and pith studied in this paper, and the other parameters cannot be determined directly due to the limitation of the test equipment or the problem of the testing technology, and the combination of the composite material theory and the comparative method was used here to make the selection. According to the composite material theory, it was known that the following relationship exists between the elastic modulus and Poisson's ratio of orthotropic anisotropic materials:

$$\begin{cases} \dfrac{\mu_{21}}{\mathrm{E}_1}=\dfrac{\mu_{12}}{\mathrm{E}_2} \\ \dfrac{\mu_{31}}{\mathrm{E}_1}=\dfrac{\mu_{13}}{\mathrm{E}_3}\Rightarrow\dfrac{\mu_{ij}}{\mathrm{E}_j}=\dfrac{\mu_{ji}}{\mathrm{E}_i} \quad (i,\ j=1,\ 2,\ 3;\ i\neq j) \\ \dfrac{\mu_{32}}{\mathrm{E}_2}=\dfrac{\mu_{23}}{\mathrm{E}_3} \end{cases} \tag{1}$$

From the above equation (1), only six of the nine engineering constants are independent. Within the isotropic surface, the modulus of elasticity E, Poisson's ratio μ, and shear modulus G (1, 2, and 3 for the x, y, and z directions, respectively) also satisfy the simple relationship in the theory of elasticity(He et al. 2024). Based on actual biomaterial studies, the numerical ratios are still quantitatively related within non-isotropic surfaces, as shown in equation (2, 3):

$$G=\frac{E}{2(1+\mu)} \tag{2}$$

$$G_{ij}=(\frac{1}{3}\sim\frac{1}{2})E_{ij}\ (i,j=1,2,3;\quad i\neq j) \tag{3}$$

From agricultural biomechanics, it was known that the Poisson's ratio of the majority of materials was between 0.2 and 0.5, and for isotropic materials, the Poisson's ratio was generally around 0.3. Referring to the relevant(Li et al. 2018. Qin et al. 2011) literature to establish the intrinsic model, the selected parameters of reed straw bark and pith were as follows**Table 1** was shown in Table 1.

Table 1 Definitions of elastic parameters for finite element analysis of reed straw.

Elastic parameter	Reed straw	
	Surname Pi	Pith (soft interior of plant stem)
E_x /MPa	2514.60	44.24
E_y /MPa	2514.60	44.24
E_z /MPa	8812.40	249.32
G_{xy} /MPa	1884.30	22.42
G_{xv} /MPa	4573.58	122.70
G_{yv} /MPa	4573.58	122.70
μ_{xy}	0.25	0.030
μ_{xv}	0.18	0.0020
μ_{yv}	0.18	0.0020

3.3.2 Grid division and loading conditions

After saving the simplified model of the reed straw as an IGS file, it was imported into HyperMesh for meshing, and the mesh model was subsequently exported. The material properties, cross-sectional properties, boundary conditions, and load conditions were then defined. Given that the stalks analyzed in this study exhibit axial symmetry and that the fibers are aligned along the axial direction, hexahedral cells were chosen for meshing along the axial direction. Additionally, the three-dimensional solid element SOLID186 was selected for the mesh. A network division method was applied, and the cell size was set to 0.05 mm. The geometric shape of the reed stalks is regular, and the mesh quality, including the number of grid cells, the sparsity of the grid cells, and the overall grid quality, were assessed. These parameters are presented in Table 2.

Table 2 Straw model grid and number of cells.

Measurement object	Number of nodes		Number of units	
	Simplified model	Real model	Simplified model	Real model
Rind	20194	24880	60515	78563
Foam matrix	30349	61221	133095	122972
Fibres	-	42000	-	62400

According to the compression analysis of the model, the stem intercepted section fails at axial and radial compression up to 25% under the mechanical universal testing machine, i.e. exceeding the strain limit of elastic deformation, and therefore only compressed up to 20% here.

4 ANALYSIS OF STRAW MACRO-MICROSTRUCTURE AND SIMULATION RESULTS

4.1 Microanalysis of reed straw vascular bundles

Reed straw was composed of an outer bark, basic tissues and vascular bundles. Among them, vascular bundles are scattered in the basic tissues and their microstructure was shown in**Erro! Fonte de referência não encontrada.** .The microstructure of vascular bundles was shown in Figure 5. The size of vascular bundles gradually increased and their number decreased from the outside to the inside of the reed straw. Large vascular bundles were mainly distributed in the outer region of the straw (**Erro! Fonte de referência não encontrada.**A, B), while small vascular bundles were predominantly distributed in the inner region (**Erro! Fonte de referência não encontrada.**C, D). The basic organisation of the straw pith core had a foamy chamber structure, and the pith core was relatively homogeneous in texture, with its foamy matrix organisation completely filling the outer bark. The outer bark appeared stepped thickening and epithelialisation at nodes, and the close apposition of the foamy basic tissue to the outer bark (**Erro! Fonte de referência não encontrada.**E, F).

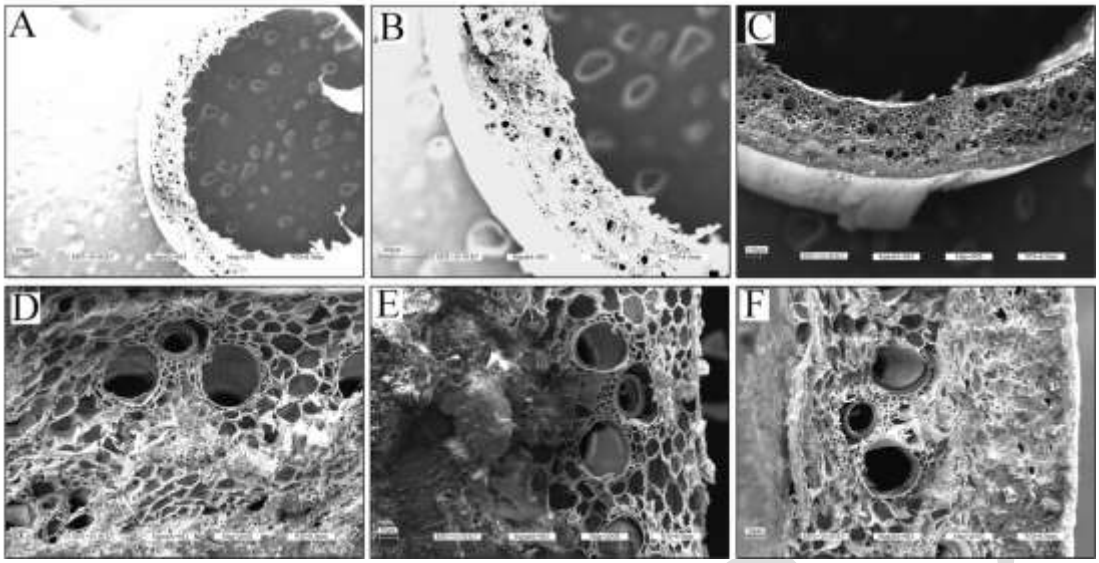

Figure 5 *Microstructure of reed straw (A-B): tightly bound outer epidermis and pith core; (C-D) hollow structure of small vascular bundles; (E-F) hollow structure of large vascular bundles.*

4.2 Analysis of simulation results

4.2.1 Axial Compression Simulation

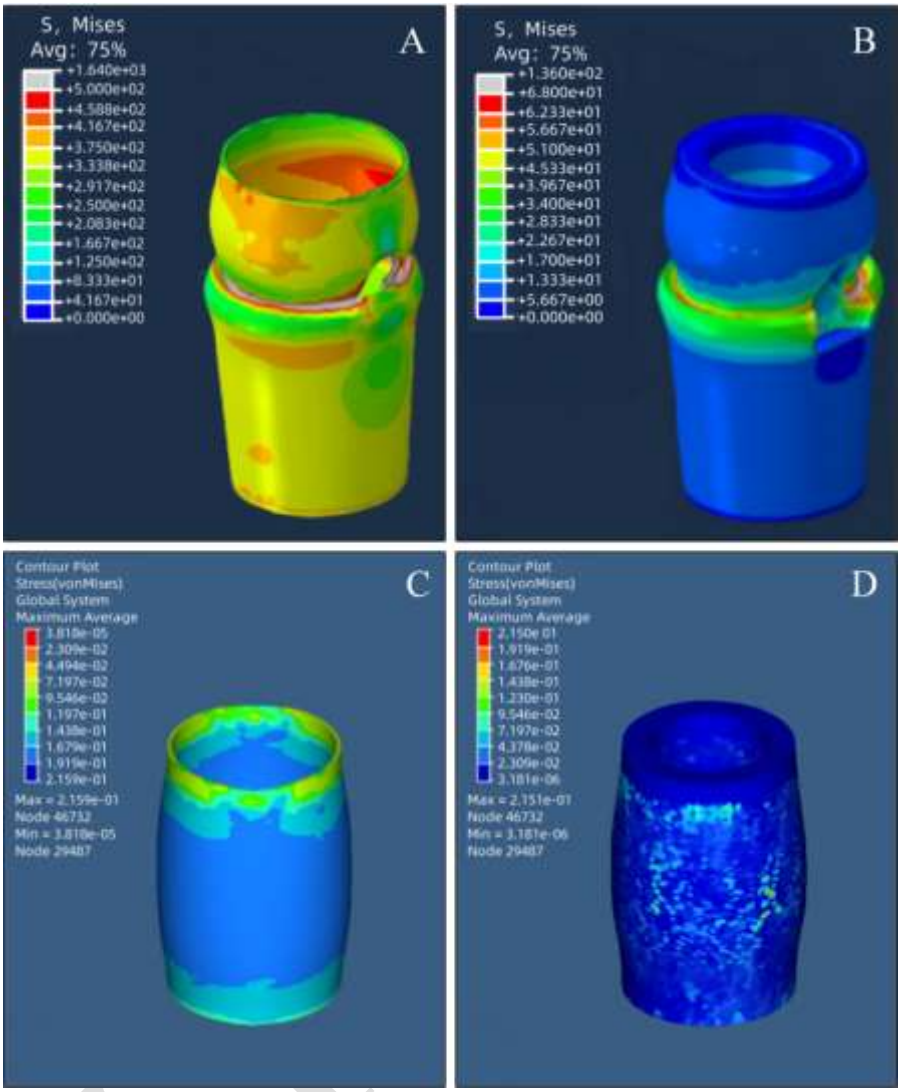

Figure shows the deformation and stress cloud of the reed straw model during axial compression. Since the cross section of the straw is nearly circular, the stress distribution was more uniform. The maximum value of the stress occurs at the upper part of the node. The stresses in the upper contact part are greater than the lower part, indicating that the straw was more prone to failure in the upper part, which was consistent with the deformation during mechanical testing.

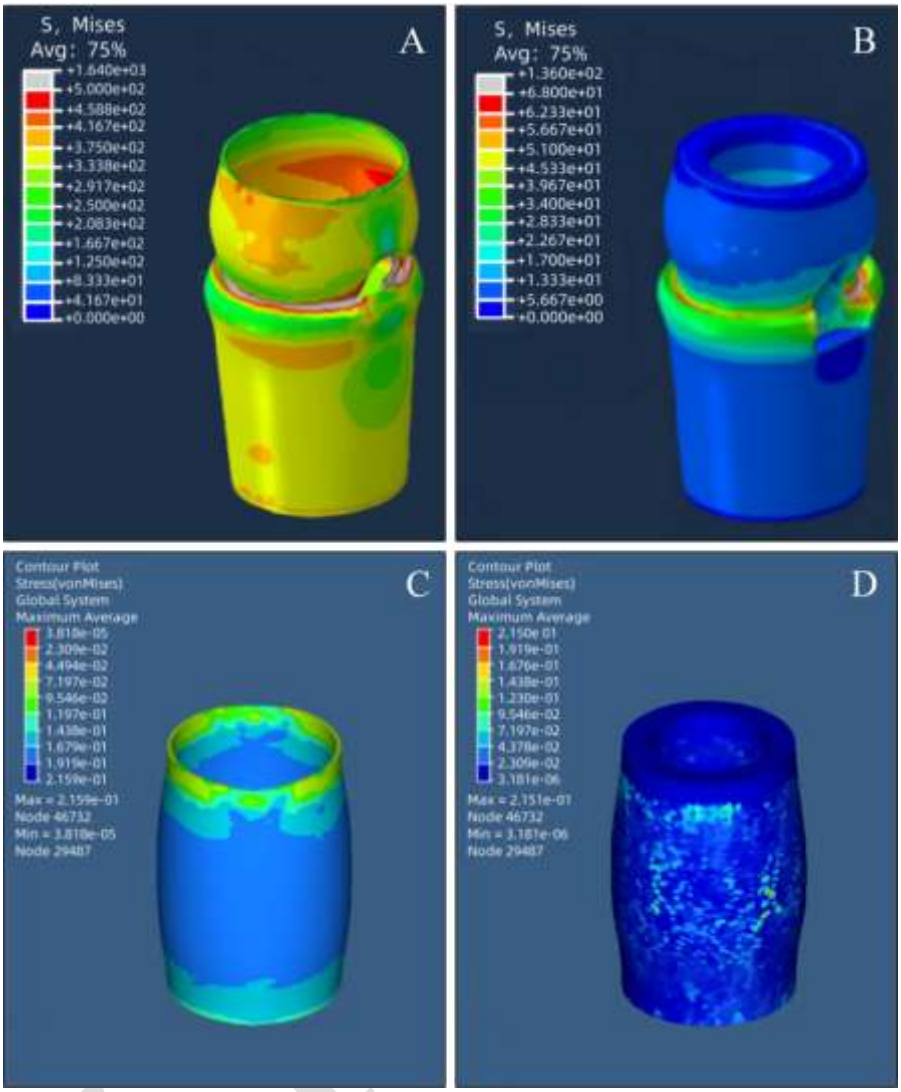

Figure A) Stress diagrams with grey area at the upper position at the node, where the stress value was the highest at 1640 Mpa, indicating that the strength was close to failure at this location. The stress distribution of the medullary core was similar to that of the epidermis, with the maximum value also appearing at the node, while the stress distribution of the upper and lower parts of the node was more uniform, indicating that the foam structure at the node was radially constrained by the external epidermal node features, as shown in

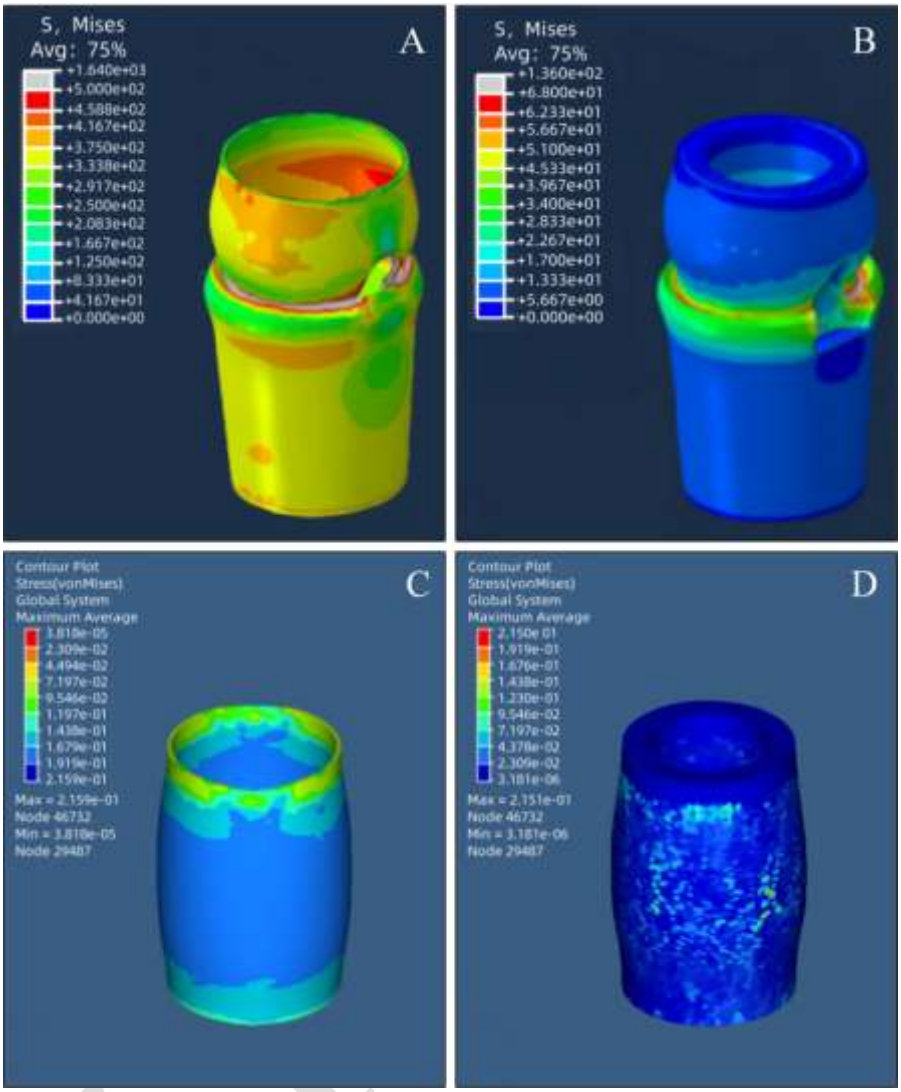

Figure B) shows. Compared with the real model, the stress distribution of both the epidermis and the pith core on the simplified model was more uniform, as shown in

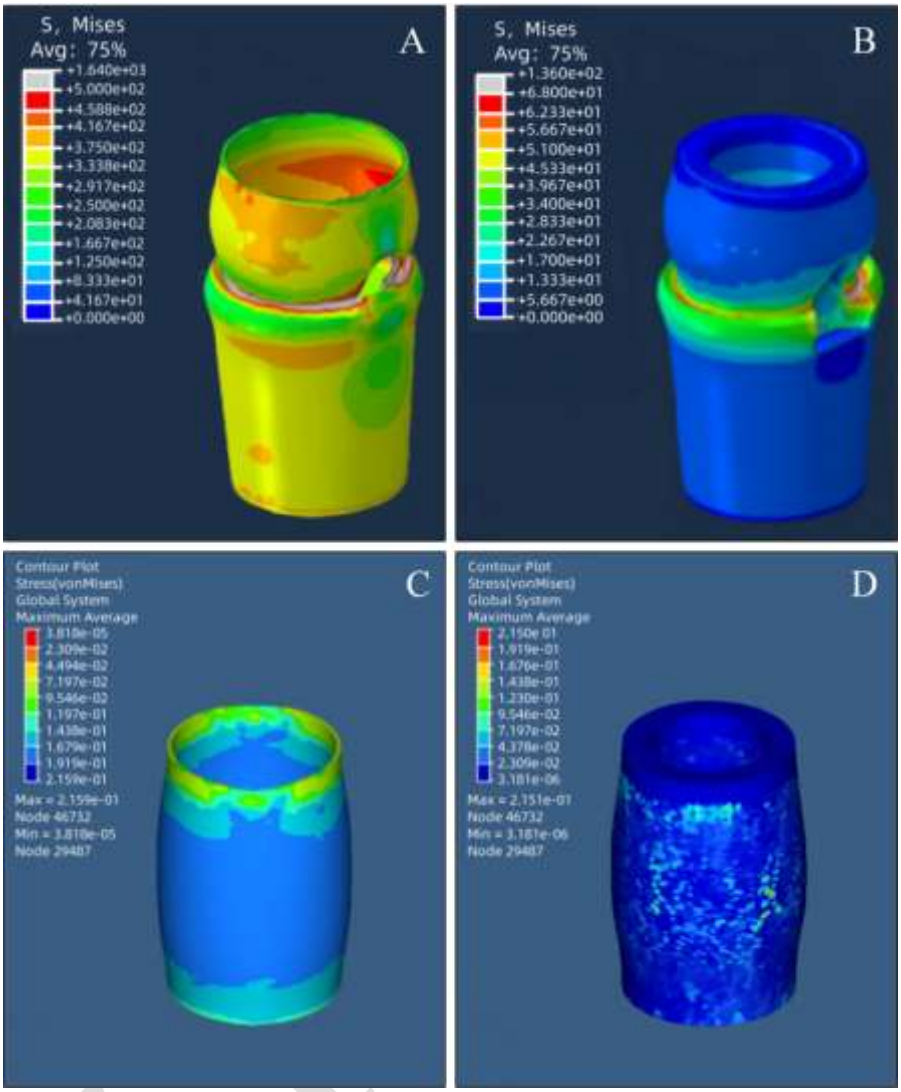

Figure C, D) shown. The difference was that under the same failure stress criterion, no obvious failure point was seen in the simplified model.

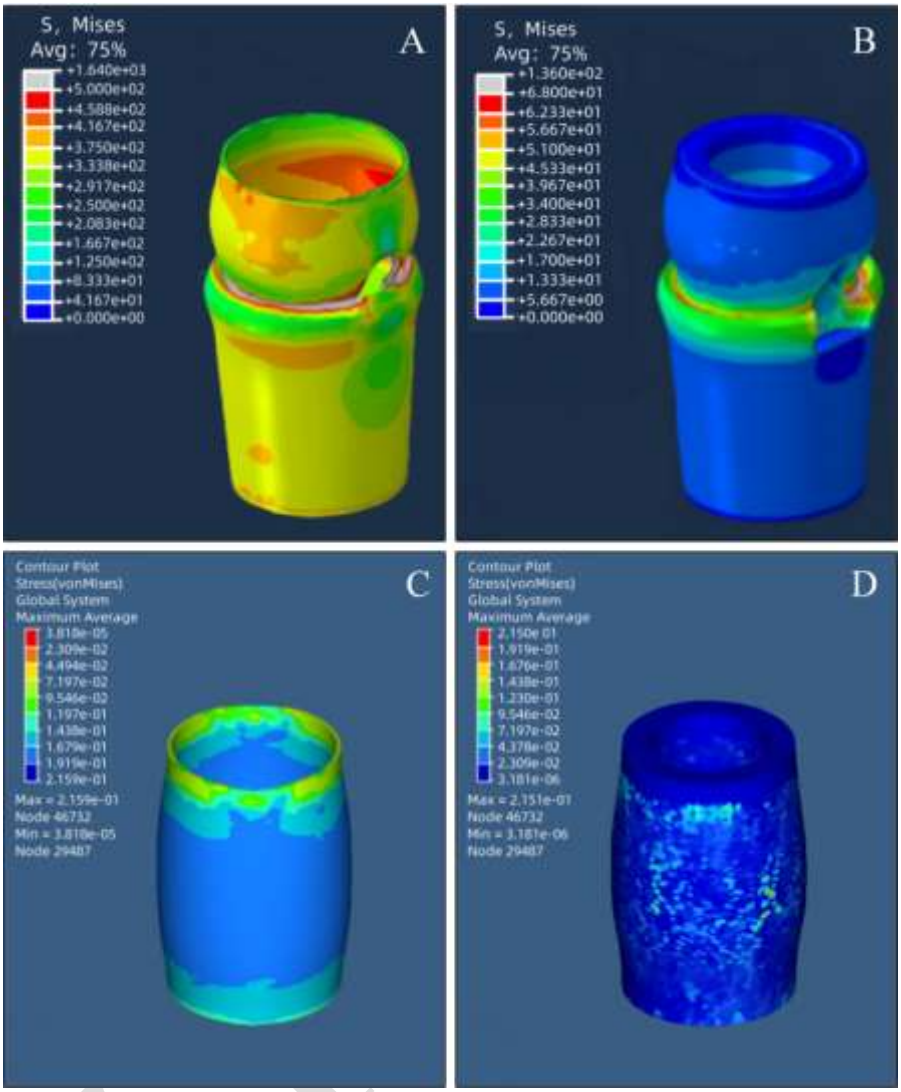

Figure 6 *Reed straw axial compression deformation and stress cloud; (A) real reconstruction model of the epidermis, (B) real reconstruction model of the pith core, (C) simplified model of the epidermis, (D) simplified model of the pith core.*

4.2.2 Radial compression simulation

Figure 7 presents the deformation and stress distribution diagrams for the two models of reed straw under radial compression. For reed straw, the stress distribution under radial compression is characterized by inhomogeneity, with higher stresses observed in the epidermis compared to the pith core. Since the circular structure at the nodes was a complete circle, the stresses are distributed in the form of strips along the growth direction, and no significant rendezvous occurs. The maximum stress value also occurs at the node and reaches about 619 MPa, and multiple stress failures occur at the node off the upper indenter site, which was consistent with the deformation during the mechanical tests. Since the pith core was a porous structure, it was not easy to be damaged and the stress distribution was more uniform. Same as the outer skin, the stresses showed a bar-shaped distribution along the growth direction, as shown in***Figure*** B) shows. Comparing with the real model, since the structure was a regular two-circle structure, the stress distribution was also more uniform, and the same bar-shaped stress distribution occurs at the strain maximum, which reaches 54.86 Mpa as shown in***Figure*** C,D) shown. The difference was

that under the same failure stress criterion, no obvious failure point was seen in the simplified model.

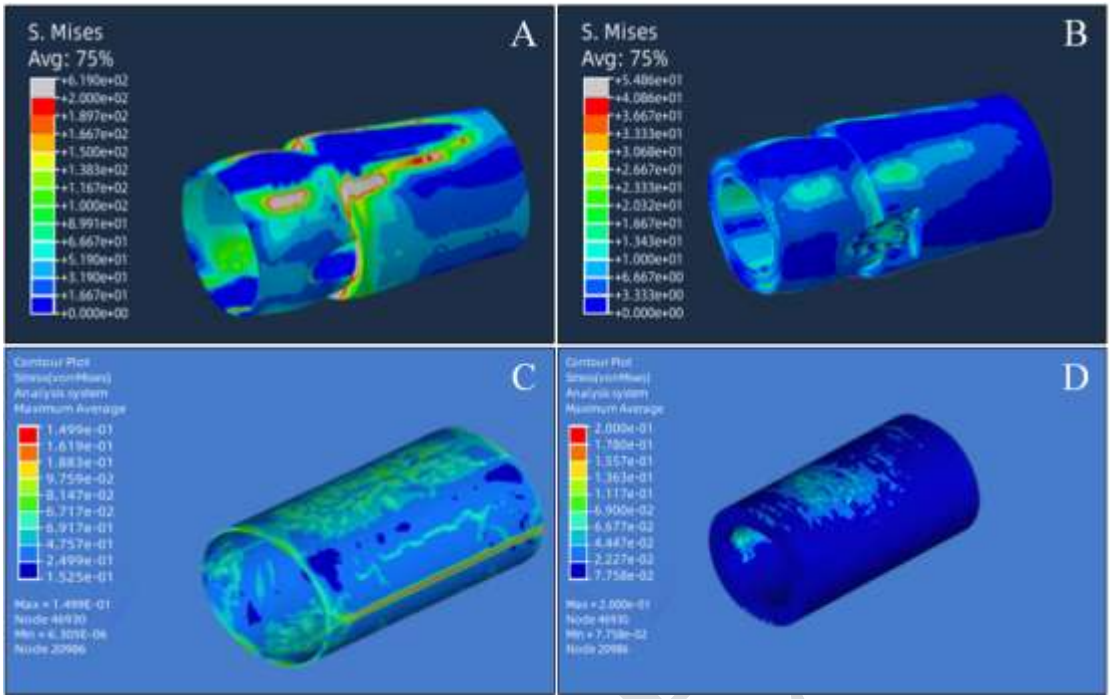

Figure 7 *Radial compressive deformation and stress cloud of reed straw: (A) real reconstruction model of the epidermis; (B) real reconstruction model of the pith core; (C) simplified model of the epidermis; (D) simplified model of the pith core.*

According to the maximum strain strength criterion for orthotropic materials, failure occurs when strain exceeds the material's ultimate strain. In the simulation results of the real reconstruction model, skin stress failure was observed, which aligned with the experimental results. During transverse compression, the strain increased sharply from the pith to the outer skin due to the lower elastic modulus of the pith compared to the skin. The strain at the skin reached its maximum, and because the skin is composed of axially arranged fibers with weaker transverse bonding, reed straw is more prone to fracture during radial compression.

Table 3 shows the simulated and experimental test values for the simplified and real models.. The simulated values of axial and radial compression of reed straw were generally higher than the experimental values because the intrinsic model of fracture was not considered in the simulation analysis. Among them, the maximum error of the simplified model was 22.15% and the minimum error was 16.67%. While the maximum error of the real model was 14.33% and the minimum error was 10.77%.

Table 3 Simulation stress values.

Compression method	Test items	Straw stress value
Axial compression	Experimental model value/MPa	57.59
	Simplified model-simulated value/MPa	68.93
	Simplified model - simulated value - error/%	19.07
	Real model-simulated value/MPa	64.59

	Real model - simulated value - error/%	12.16
	Experimental test value/MPa	1.02
	Simplified model-simulated value/MPa	1.25
	Simplified model - simulated value - error/%	22.15
Radial compression	Real model-simulated value/MPa	1.17
	Real model - simulated value - error/%	14.33

4.3 Structural analysis of reed stem nodes

Based on the results of the aforementioned simulation analyses, the nodal features demonstrate a significant enhancement in the axial and radial compression behavior of straw, highlighting their crucial role in maintaining structural stability. Therefore, conducting an in-depth analysis of the mechanical behavior of straw with nodes under radial loading conditions is of considerable importance. Both in axial and radial compression, the nodal features effectively contribute to structural stability by providing radial constraints to the outer epidermis and pith core of the straw. Consequently, this study focuses on the force characteristics of straw with nodes under radial compression.

The cross-section of the reed straw was shown inReed straw also has a very complex structure, with a complex straw structure characterised by a distinct vascular vascular structure and obvious discontinuities on a microscopic scale(Mazzol et al. 2024. Kou et al. 2024).

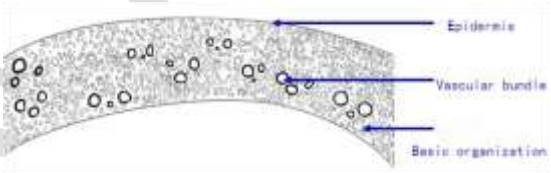

All of them are mainly composed of epidermis, mechanical tissues and basic tissues distributed with vascular bundles, but differ in the combination of vascular bundles and their size classes.

Reed straw also has a very complex structure, with a complex straw structure characterised by a distinct vascular vascular structure and obvious discontinuities on a microscopic scale(Mazzol et al. 2024. Kou et al. 2024).

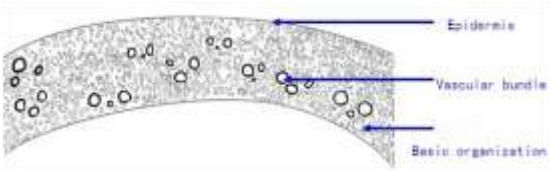

Figure 8 *Cross-section of straw: reed straw.*

In order to establish a computational model suitable for mechanical research and analysis, simplifying assumptions needs to be made about the straw material. Firstly, discontinuities and

their defects in the fine structure of the material are ignored and a tight connection between the parts of the material was assumed to simplify the model. Secondly, the interlayer misalignment was not considered so that the displacement continuity condition can be easily applied. In addition, the material was assumed to have transverse isotropic properties and the viscous behaviour of the material was ignored. Finally, it was assumed that the fibres inside the material are all neatly aligned along the axial direction, thus simplifying the mechanical description of the material parts.

As shown in**Erro! Fonte de referência não encontrada.** 9, the formula for the critical buckling force of the knuckle diaphragm can be deduced with a diaphragm radius of r and a thickness of t.(Botis et al. 2022. Florin et al. 2022) It was assumed that the circumferential edges of the knuckle diaphragm are fixed to the inner surface of the straw, and that the stem was subjected to a uniform pressure *q*. Under the load in the transverse direction, the knuckle diaphragm will be bent and a rotationally deformed surface will be generated. The knuckle diaphragm was characteristically subjected to orthogonally distributed compressive and tensile stresses, and the critical flexion force of the knuckles was shown in the Figure 9.

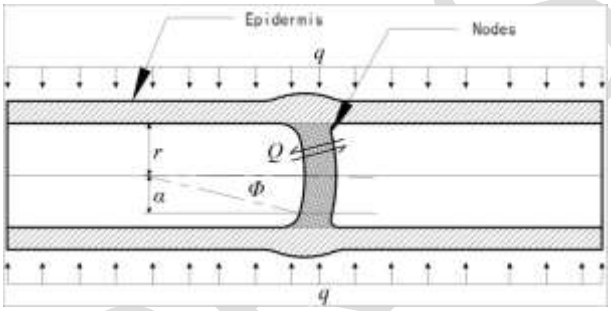

Figure 9 *Schematic diagram of radially homogeneous compression loads on reed straws.*

Defining *Φ* as the angle between the rotation axis of the nodal diaphragm and the surface normal, and α denotes the distance from the centre of the nodal diaphragm to any point on the inner surface, the differential equation for the deformed equilibrium state of the nodal diaphragm as shown in equation (4):

$$\alpha^2 \frac{d^2\phi}{d\alpha^2} + \alpha \frac{d\phi}{d\alpha} - \phi = -\frac{Q\alpha^2}{D} \tag{4}$$

Q was the shear force per unit length and *D* was the flexural stiffness of the tissues that make up the knuckle diaphragm. Assuming that there was no lateral load acting on the knuckle diaphragm, the critical buckling force F_c was given by equation (5).

$$F_c = \frac{Q}{\phi} \tag{5}$$

$$\gamma^2 = \frac{F_c}{D} \tag{6}$$

Combining equations (4) through (6), the equilibrium equation can be expressed as shown in equation (7). By introducing the new variable $u=\gamma r$, this equation can be greatly simplified, resulting in equation (8):

$$\alpha^2 \frac{d^2\phi}{d\alpha^2} + \alpha \frac{d\phi}{d\alpha} + \phi(\gamma^2 r^2 - 1) = 0 \tag{7}$$

$$u^2 \frac{d^2\phi}{du^2} + u \frac{d\phi}{du} + \phi(u^2 - 1) = 0 \tag{8}$$

Because the general solution of the second order equation of such a formula is as follows in equation (9):

$$\phi = A_1 J_1(u) + A_2 Y_1(u) \tag{9}$$

A_1 and A_2 are constants and $J_1(u)$ and $Y_1(u)$ are first-order Bessel functions of type I and type II, respectively, from the boundary conditions $\alpha = r = 0$ and $\phi = 0$ at the centre of the nodal diaphragm. It can also be seen that $A_2 = 0$, although $Y_1(u)$ tends to infinity when $u = \gamma r$ tends to 0. Also, the equilibrium condition at the deformed edge of the nodal diaphragm must be satisfied with $\alpha = r$ and $(\varphi)_{r+a} = 0$ making $J_1(\gamma r) = 0$. The smallest root of $J_1(\gamma r) = 0$ is $\gamma r = 3.832$. Substituting this value into equation (6), and shows that in equation (10):

$$\frac{F_c}{D} = \gamma^2 = (\frac{3.832}{r})^2 = \frac{14.68}{r^2} \tag{10}$$

It follows that equation (11)

$$F_c = \frac{14.68D}{r^2} \tag{11}$$

For a knuckle diaphragm structure, the flexural stiffness is equal to $\frac{Et^3}{12(1-\upsilon^2)}$, where E is the Young's modulus of elasticity, t is the thickness of the diaphragm and υ is the Poisson's ratio. Therefore, the critical buckling force of a sectional diaphragm was given by the following equation (12):

$$F_c = \frac{14.68Et^3}{12(1-\upsilon^2)r^2} \approx \frac{1.2Et^3}{(1-\upsilon^2)r^2} \tag{12}$$

From equation (12), it can be seen that there is a power positive correlation function relationship between the critical buckling force and the diaphragm thickness t, i.e., the larger the wall thickness is, the stronger the radial reinforcement of its nodes; on the other hand, it multiplies a quadratic negative correlation function relationship with the radius of the stem, i.e., the larger the direct of the stem is, the weaker the radial reinforcement of the nodes is. Therefore, the relationship between the thickness of the node and the radius of the stalk can be balanced in the mechanical analysis to optimise the load-bearing capacity of the stalk structure. This further highlights the important role played by node characteristics in the process of radial constraint and load-bearing of stalks.

5 CONCLUSION

In this study, the structure of reed straw was reconstructed in three dimensions using Micro-CT and Mimics inverse reconstruction techniques. The resulting 3D model, combined with the material properties of the stalks, enabled a detailed analysis of the mechanical behavior of reed straw under axial and radial compression conditions through finite element analysis. The model's results were then compared with experimental test data. The force characteristics of the nodal diaphragm were discussed in detail, and the key conclusions are summarized as follows:

A detailed digital model of the reed straw structure was developed using Micro-CT and Mimics inverse reconstruction techniques. In comparison with traditional models, this model more accurately captures the conical shape of the straw, as well as the nodal features. It also includes detailed representations of the outer sheath wall structure and the inner vascular bundle structure.

Due to the complex nature of the ontological relationship for anisotropic materials, certain elastic constants could not be directly determined. Therefore, the elastic constants for the straw cortex and pith core were determined separately using a comparative selection method, which incorporated the characteristics and parameters of biological materials. Subsequently, a finite element simulation and analysis model of reed straw was established.

(3) The equivalent force clouds of the pith core and outer skin were derived by finite element simulation of nodded reed straw under axial and radial loads. The results show that the maximum error of the simplified model is 17.32% and the minimum error is 22.15%, while the maximum error of the real model is 14.33% and the minimum error is 10.77%.

(4) The strengthening effect of the straw node structure was analysed, the force analysis model of straw with nodes was established, and the critical buckling stress formula applicable to the compression of the middle node structure of reed straw was theoretically deduced.

6 EXPECTATIONS

Future Research Directions and Recommendations

Heterogeneous Material Modeling: Future studies should incorporate advanced material modeling that accounts for the heterogeneity of reed straw, including variations in the epidermis, pith core, and vascular bundles. Multi-scale modeling, integrating microscopic and macroscopic properties, would improve predictions of local stresses and deformations.

Non-linear Behavior and Damage Models: The current study assumes linear elasticity, but reed straw may exhibit non-linear behavior and damage under large deformations. Incorporating plasticity, fracture mechanics, and damage models could enhance the accuracy of simulations, especially near failure points.

Experimental Validation and Stress Distribution: High-resolution experimental techniques like digital image correlation (DIC) or X-ray tomography could validate the internal stress distributions from simulations. Testing under dynamic loading (cyclic or impact loads) would provide insights into reed straw's behavior in real-world conditions, such as wind or vibration.

Effect of Environmental Factors:

Seasonality and Moisture Content: Future research should explore the impact of moisture absorption and seasonal changes (e.g., fiber alignment, vascular bundle distribution) on the mechanical properties of reed straw.

Long-term Durability: Investigating the long-term performance of reed straw under environmental conditions like UV exposure, humidity, and biological degradation will provide insights into its durability and sustainability for industrial use.

Optimizing Reed Straw for Engineering Applications: Research could focus on optimizing reed straw's mechanical properties by manipulating growth conditions (e.g., harvesting times, growth rates). Structural optimization for use in bio-composites or lightweight construction materials could further enhance reed straw's utility.

Simulation Accuracy and Computational Methods: The accuracy and efficiency of FEM models could be improved by using higher-resolution models and mesh refinement techniques. Parallel computing and machine learning algorithms could also optimize simulations for real-time performance predictions.

Bio-Inspired Design and Material Innovation: The unique structural features of reed straw, particularly its node structure and vascular bundle arrangement, offer potential for bio-inspired materials. Future research could explore how these natural characteristics could be applied in designing lightweight structures or self-healing materials.

This study provides valuable insights into the mechanical behavior of reed straw, but further research is needed to refine computational models, assess environmental influences, and explore the optimization of reed straw for industrial applications. These efforts will not only enhance our understanding of reed straw's properties but also expand its potential use in sustainable engineering and design.

Author's Contribuitions:

Editor: Pablo Andrés Muñoz Rojas

References

Cheng, Y. Hu, H. Di, Y. (2013).Analysis of the Impact of Straw Returning on Soil and the Current Status of Straw Returning in Anhui Province .Agricultural Science & Technology.14(5):776-779.

Feng, W. Zhang ,L. He, L. (2011). Research on the Utilization Model of Crop Straw Resources Based on Circular Agriculture. Agricultural Science and Technology (English version). 12 (12): 1921-1924.

Yin Q ,Yu M ,Ma X .(2023). The Role of Straw Materials in Energy-Efficient Buildings: Current Perspectives and Future Trends. Energies. 16(8).

SHON, C, S. MUKASHEV, T. LEE, D. (2019). Can common reed fibre become an effective construction material?Physical,mechanical,and thermal properties of mortar mixture containing common reed fiber. Sustainbility.11 (3):903.

Song J ,Xu S ,Xu L .(2020). Experimental study on the crashworthiness of bio-inspired aluminium foam-filled tubes under axial compression loading.Thin -Walled Structures,155.

RISÉN E,GREGEBY E,TATARCHENKO O. (2013). Assessment of biomethane production from maritime common reed. Journal of Cleaner Production. 53:186 -194.

O Dogherty M J , Huber J A , Dyson J . (1995). A Study of the Physical and Mechanical Properties of Wheat Straw. Research. 62(2):133-142.

Wang,S, Zhang,B, Li,X. (2018). Experimental study on mechanical properties of fresh corn straw.

S. Regragui, M. Bousfia, F.-E. El Mabchour, M. Taha Janan, M. Aboussaleh and E. M. Zemmouri. (2023). Computation of Mechanical Properties of Earthen Matrix Reinforced by Straw Fibers Using 3D Modeling. International Conference on Digital Age & Technological Advances for Sustainable Development. Casablanca, Morocco pp, 67-72.

Bavan S D ,Kumar M C G .Finite (2013). Element Analysis of a Natural Fiber (Maize) Composite Beam.Journal of Engineering,20131-7.

Song J ,Li G ,Liu Y. (2024). Comparative Analysis of Macro/Microstructures and Constituents of Sorghum and Reed Straw. Biomimetics,9(2):107.

Han, S., He, Y., Ye, H. (2024). Mechanical Behavior of Bamboo, and Its Biomimetic Composites and Structural Members: a Systematic Review Bionic Eng 21, 56 J Bionic Eng 21, 56 -73 .

Fu D , Liu Z , Yang W L S .(2023). EXTRACTION AND CHARACTERIZATION OF NATURAL CELLULOSE FIBERS FROM REED STRAW: MORPHOLOGICAL, MICROSTRUCTURAL AND THERMAL PROPERTIES. Cellulose Chemistry and Technology: International Journal for Physics, Chemistry and Technology of Cellulose and Lignin.

Ali E ,Chenchen P ,Ruiyao C. (2016). Whole organ and organism tissue clearing by uDISCO.Protocol Exchange.

Li, A. Kingston, G. Myers, B. Recur and A. Sheppard,(2015) 3D X-Ray Source Deblurring in High Cone-Angle Micro-CT, in IEEE Transactions on Nuclear Science, vol. 62, no. 5, pp. 2075-2084.

Luo L ,Qu Q ,Lin H.(2024). Exploring the Evolutionary History and Phylogenetic Relationships of Giant Reed (Arundo donax) through Comprehensive Analysis of Its Chloroplast Genome[J].International Journal of Molecular Sciences 25(14):7936-7936.

Huang, J., Yang, Y., Zhou, F.(2023) Biomechanical stability variation of rice stem during maturation and wilting.Journal of the Brazilian Society of Mechanical Sciences and Engineering,2023,45(2):

Yan M ,Song C ,Wanping L. (2024) Exploring approaches to tackle cross-domain challenges in brain medical image segmentation: a systematic review. Frontiers in Neuroscience,181401329-1401329.

Schwaiger M ,Bender M ,Schirmer H. (2024). Effect of different weft-knitted structures on the mechanical performance of bio-based flexible composites.Composites Part C: Open Access,13100436.

Yi Q, Zhen Y, Bai J. (2024). Modified Differential Quadrature Method Using Basis Functions Satisfying Multiple Boundary Conditions for Buckling Analyses of Beams and Rectangular Plates.Journal of Engineering Mechanics,150(8).

Yan B ,Liu H ,He F . (2024) Analysis and Testing of Pre-Cut Sugarcane Seed Stalk Sawing Performance Parameters.Agriculture,14(6):953-953.

Ingrīda A ,Anda L ,Ingmārs C . (2021). Phenolic Compounds in Organic and Conventional Winter Wheat (Triticum aestivum L.) Wholemeal. Proceedings of the Proceedings of the Latvian Academy of Sciences. Section B. Natural, Exact, and Applied Sciences.,75(6):444-448.

EWA G G C A M. (2011). MECHANICAL AND ACOUSTIC PROPERTIES OF SPRING WHEAT VERSUS ITS TECHNOLOGICAL QUALITY FACTORS.Journal of Texture Studies,42(4):319-329.

Kuai B ,Qiu X ,Zhan T. (2024). Optimization of mechanical properties and dimensional stability of densified wood using response surface methodology. International journal of biological macromolecules,273(P1):132958-132958.

Tamás K ,Földesi B ,Rádics P J. (2015). A Simulation Model for Determining the Mechanical Properties of Rapeseed using the Discrete Element Method. Periodica Polytechnica Civil Engineering,59(4):575-582.

He J ,Sun C ,Wang X .(2024). Mechanical Properties and Microanalytical Study of Concrete Reinforced with Blended Corn Straw and Scrap Steel Fibers. Materials (Basel, Switzerland),17(15):3844-3844.

Y. Li, J. Wang, X. Qiu, Y. Ge, J. Zhang and Y. Pu.(2018). Study on the Compressive Mechanical Properties of Greenfeed Sweet Sorghum. 2018 3rd International Conference on Mechanical,pp. 10-15

Mazzoli M ,Scarpolini A M ,Fanni M B. (2024). An AI and Statistical Shape Analysis combined framework to extract features in complex cardiovascular structures. Vascular Pharmacology, 155107331-107331.

Kou G ,He K ,Yang M. (2024). Multiscale verification method for prediction results of mechanical behaviours in unidirectional fiber reinforced composites. Composites Part A,186108387-108387.

Botis, M. F., & Cerbu, C. (2022). Design Solutions for Slender Bars with Variable Cross-Sections to Increase the Critical Buckling Force. Materials, 15(17), 6094.

Florin M B ,Camelia C . (2022). Design Solutions for Slender Bars with Variable Cross-Sections to Increase the Critical Buckling Force.Materials,15(17):6094-6094.